2019-09-06

Non-iterative parameter estimation of the 2R-1Cmodel suitable for low-costembedded hardware

MItar Simić, Zdenka Babić, Vladimir Risojević, Goran Stojanović

springerlink

MItar Simić, Zdenka Babić, Vladimir Risojević, and Goran Stojanović. 2019. Non-iterative parameter estimation of the 2R-1Cmodel suitable for low-costembedded hardware. Frontiers of Information Technology & Electronic Engineering 2019(6): 1–6. doi: https://doi.org/10.1631/FITEE.1900112.
https://open.uns.ac.rs/handle/123456789/9642

Circuits, Systems, and Signal Processing manuscript No.
(will be inserted by the editor)

Non-Iterative Parameter Estimation of the 2R-1C Model Suitable for Low-Cost Embedded Hardware

Mitar Simić · Zdenka Babić · Vladimir Risojević · Goran M. Stojanović ·

Received: date / Accepted: date

Abstract Parameter estimation of the 2R-1C model is usually done with iterative methods which increases required complexity of measuring and data processing units. Because of that there is a strong motivation to develop methods for faster and power efficient parameter estimation with low-complexity algorithms suitable for microcontroller-based devices. Such approach is more applicable for practical use when low-cost and nearly real-time estimation are needed. In this paper we present the non-iterative approach based on quadratic interpolation for characteristic frequency estimation from imaginary part of measured impedance, while the 2R-1C model parameters are calculated based on the set of analytical expressions. Analysis with impedance data of the 2R-1C model, obtained by simulation and measurement, showed that the approach with quadratic interpolation can reduce required number of measurement points for 80% in comparison with previously reported the non-iterative approach without quadratic interpolation, but to keep estimation error lower than 1%, too. Approaches with and without quadratic interpolation were implemented on the microcontroller-based device for comparison regarding the estimation accuracy, RAM and flash memory usage as well as the execution time. Experiments showed that addition of quadratic interpolation introduces slightly higher execution time (about 6.7%), requires 24% more flash memory and just 2.4% more RAM. However, root mean square errors for calculated impedance with model parameters estimated using quadratic interpolation are

Mitar Simić, Zdenka Babić and Vladimir Risojević
University of Banja Luka,
Faculty of Electrical Engineering
Patre 5, 78000 Banja Luka, Bosnia and Herzegovina
E-mail: {mitar.simic, zdenka.babic, vladimir.risojevic}@etf.unibl.org

Goran M. Stojanović
University of Novi Sad
Faculty of Technical Sciences
Trg Dositeja Obradovića, 21000 Novi Sad, Republic of Serbia
E-mail: sgoran@uns.ac.rs

smaller for 42.8% (real part) and 51.5% (imaginary part) in comparison with estimation without quadratic interpolation.

Keywords 2R-1C model · parameter estimation · quadratic interpolation

1 Introduction

Non-destructive techniques (electrical impedance spectroscopy, dielectric spectroscopy, thermal imaging, eddy current testing, magnetic particle or radiographic and ultrasonic methods, etc.) for evaluation of properties of materials, processes and structures have been a topic of high importance and interest in scientific community. For example, electrical impedance spectroscopy is a powerful and widely used technique in many fields as a method for unraveling complex non-linear processes for many material-material interfaces and applications. Measured electrical impedance as a function of the excitation frequency can reveal internal dynamics or underlying processes [22]. It is possible to present different material-material interfaces, structural characteristics and internal connections with corresponding basic electrical elements such as resistors (R), inductors (L) or capacitors (C) to form equivalent electrical circuit (model). In literature, electrical circuits are widely reported as approach in modeling of sensors [42, 43], biological cells and bioimpedance [30, 35], solar cells [20], proton exchange membrane (PEM) fuel cells [44], batteries [12, 27] as well as in unsteady heat transfer analysis [45] and prediction of total body water volume [16].

Structure of the equivalent electrical circuit is usually chosen based on the previous knowledge of internal structure and involved physical processes. Parameter estimation is focused on finding values of model parameters which ensure low difference between measured impedance and impedance calculated with extracted values of model parameters. Increasing power of available computing units, allows use of very complex models containing empirical elements such as constant phase element (CPE) and the Warburg diffusion element. Recently, concepts from fractional calculus (non-integer differentiation and integration) have been involved in parameter estimation of equivalent electrical circuits [2, 15, 26]. However, many electrochemical processes have inherently capacitive electrical behavior which in modeling permits use of simple R-C models rather than complex models [12, 16, 20, 23–25, 27, 30, 35, 42–45]. The 2R-1C model, which consists of two resistors (R_1 and R_2) and one capacitor (C_2), with connections shown in Fig. 1, is widely used because of simplicity and ability to have direct physical interpretation of model parameters [34].

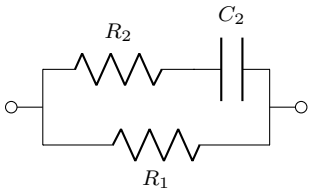

Fig. 1 The 2R-1C model.

For example, in bioimpedance analysis, the 2R-1C model presents biological cell where R_1 represents the resistance of the extracellular space, R_2 represents the resistance of the intracellular space and C_2 represents the capacitance of the cell membrane. In bioimpedance analysis, the Cole model of biological cell is used as well, with studies showing better accuracy in fitting the experimental high-freqeuncy impedance data compared to the 2R-1C model [48]. However, in contrast to the 2R-1C model, instead of the capacitor C_2 the Cole model contains an CPE element which does not have clear physical meaning [48]. Because of that, the 2R-1C model allows identification of changes of model parameters which represents changes in corresponding physical phenomena. For example, changes in cell membrane capacitance (C_2 in the model) reflects the characteristic features of the occurrence of many processes in the cell [4], e.g. fusion of vesicles with the plasma membrane or cell coupling via gap junctions [36], monitoring of particle uptake after cellular exposure to phagocytic stimuli [18], or cell temperature changes [19]. The 2R-1C model is used in commercial bioimpedance spectroscopy devices as well, such as ImpediMed SFB7 or Xitron Hydra 4200, which provide estimated values for the resistance of the extracellular space, the resistance of the intracellular space and the capacitance of the cell membranes from measured bioimpedance. Use of the 2R-1C model in bioimpedance analysis was reported in measuring changes in volume within an organ or whole body [14], *in-vivo* time-varying human lung tissue characterization [34], and body water volume estimation [16].

It should be emphasized that analysis of the 2R-1C circuit (Fig. 1) can be used and for alternate structure of the 2R-1C model shown in Fig. 2.

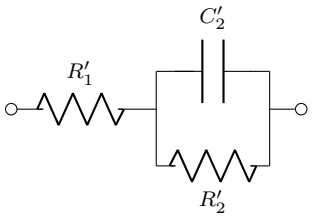

Fig. 2 The 2R-1C model formed with a resistor in series with a parallel RC circuit.

However, models from Fig. 1 and Fig. 2 have the same impedance spectra if following conditions are satisfied:

$$R_1' = \frac{R_1 R_2}{R_1 + R_2} \tag{1}$$

$$R_2' = \frac{R_1^2}{R_1 + R_2} \tag{2}$$

$$C_2' = \frac{C_2 (R_1 + R_2)^2}{R_1^2}. \tag{3}$$

In the rest of this paper we will use term 2R-1C model for the structure shown in Fig. 1, with note that complete analysis can be easily transferred to the model from Fig. 2. Moreover, as the meaning of the 2R-1C model parameters depends on the application of the model, in this paper we will consider a general case without discussion regarding physical interpretation of model parameters. Our future work is directed towards practical application of proposed method, i.e. parameter estimation from measured bioimpedance.

The complex impedance of the 2R-1C model at some angular frequency ω is given with:

$$\underline{Z}(\omega) = R(\omega) + jX(\omega) = \frac{R_1(1 + j\omega C_2 R_2)}{1 + j\omega C_2 (R_1 + R_2)} \tag{4}$$

where $R(\omega)$ and $X(\omega)$ stand for real (resistance) and imaginary part (reactance) of $\underline{Z}(\omega)$, respectively.

As the 2R-1C model consists of three parameters (R_1, R_2 and C_2) while just two measured values ($R(\omega)$ and $X(\omega)$) are available at some ω, it is not possible to have unique analytical solution of such system of equations. Iterative methods as the Taylor's polynomial [29], the Adomian decomposition method [1, 3, 10], homotopy perturbation method [17], quadrature formulas [9, 28], the Levenberg–Marquardt and the trust region algorithms in nonlinear least squares approach [6–8] are widely used in such class of mathematical problems. However, iterative methods have some limitations regarding time consumption, slow signal processing, possibility of converging towards a local minimum as well as request for high quality starting point for the values of model parameters [34]. Because of that, other approaches for parameter estimation of the 2R-1C model are continuously developed, such as differential impedance analysis [34], local polynomial method [32], use of multisine excitations instead of classical technique of frequency sweep in impedance measurement [33], and more recently fast spectral measurements and regularization [31]. However, approaches described in [31–34] are not optimized for low-cost systems with a low power processing unit because they require complex mathematical operations, thus they are typically implemented on PC-based platforms. The main contribution of this paper is formulation of the non-iterative method for parameter estimation of the 2R-1C models which is appropriate for low-cost and widely used microcontroller-based devices. Such approach ensures high system portability and reliability which is very important for practical uses where handheld devices are needed for real time estimation at the measurement site.

This paper is organized as follows: Section 2 describes non-iterative method for parameter estimation of the 2R-1C model as well as comprehensive analysis of such approach regarding estimation accuracy. Identification of parameters which can affect estimation accuracy was started with determination of influence of uncertainty in characteristic frequency on estimated values of model parameters. In addition to that, influence of number of measurement frequencies on estimation of characteristic frequency is given. Finally, the approach based on quadratic interpolation for more accurate estimation of characteristic frequency is presented. In Section 3, the main experimental results and validation of proposed method with simulated and experimentally obtained impedance data are given. The microcontroller-based implementation was analyzed regarding estimation accuracy, RAM and flash memory usage as well as execution time. Finally, the key achievements are summarized and directions of future work are described in Section 4.

2 Methods

2.1 Non-Iterative Method for Parameter Estimation of the 2R-1C Model

Real part of complex impedance of the 2R-1C model can be written as:

$$R(\omega) = \mathrm{Re}\{\underline{Z}(\omega)\} = K\frac{\omega^2 + zp}{\omega^2 + p^2} \tag{5}$$

and imaginary part as:

$$X(\omega) = \mathrm{Im}\{\underline{Z}(\omega)\} = K\frac{(p - z)\omega}{\omega^2 + p^2} \tag{6}$$

where K, z and p are defined as:

$$K = \frac{R_1 R_2}{R_1 + R_2} \tag{7}$$

$$z = \frac{1}{R_2 C_2} \tag{8}$$

$$p = \frac{1}{(R_1 + R_2)C_2}. \tag{9}$$

In our previous study the non-iterative approach for parameter estimation of 2R-1C model ($\hat{R}_1$, $\hat{R}_2$ and $\hat{C}_2$) was proposed [41]. Characteristic angular frequency ω_c of the 2R-1C model is equal to reciprocal value of time constant $\tau = (R_1 + R_2)C_2$, while first derivative of $X(\omega)$ with respect to ω is equal to zero for

$$\omega = \frac{1}{(R_1 + R_2)C_2} \tag{10}$$

which is, according to (9), equal to p. Therefore, characteristic angular frequency can be derived from the maximum magnitude of the measured imaginary part of impedance of the 2R-1C model. Our approach uses the value of

estimated characteristic angular frequency as $\hat{p}$, whereupon parameters $\hat{K}(\omega_i)$ and $\hat{z}(\omega_i)$ are calculated for each measurement angular frequency ω_i, i=1,...,N, where N is the number of data points included in the measurements, as:

$$\hat{z}(\omega_i) = \frac{R(\omega_i) \cdot \hat{p} \cdot \omega_i - X(\omega_i) \cdot \omega_i^2}{R(\omega_i) \cdot \omega_i + X(\omega_i) \cdot \hat{p}} \tag{11}$$

$$\hat{K}(\omega_i) = \frac{R(\omega_i) \cdot \omega_i + X(\omega_i) \cdot \hat{p}}{\omega_i}. \tag{12}$$

With known $\hat{p}$, $\hat{K}(\omega_i)$ and $\hat{z}(\omega_i)$, from system of equations (7)-(9), parameters of the 2R-1C model are calculated as:

$$\hat{R}_1(\omega_i) = \frac{\hat{z}(\omega_i) \cdot \hat{K}(\omega_i)}{\hat{p}} \tag{13}$$

$$\hat{R}_2(\omega_i) = \frac{\hat{z}(\omega_i) \cdot \hat{K}(\omega_i)}{\hat{z}(\omega_i) - \hat{p}} \tag{14}$$

$$\hat{C}_2(\omega_i) = \frac{\hat{z}(\omega_i) - \hat{p}}{\hat{z}^2(\omega_i) \cdot \hat{K}(\omega_i)} \tag{15}$$

for each ω_i, i=1,...,N. Finally, estimated values $\hat{R}_1$, $\hat{R}_2$ and $\hat{C}_2$ are obtained as means of $\hat{R}_1(\omega_i)$, $\hat{R}_2(\omega_i)$ and $\hat{C}_2(\omega_i)$, i=1,...,N, respectively.

Compared to iterative approaches, advantages of described method are lower computation complexity, shorter processing time, suitability for portable and autonomous low-cost microcontroller-based systems, and *in-situ* parameter estimation in real time, as well as acceptable estimation accuracy [41]. Comprehensive analysis regarding estimation accuracy and execution time showed that proposed non-iterative method in comparison with complex nonlinear least squares (Levenberg–Marquardt algorithm) was 20-80 times faster, but still providing acceptable estimation error lower than 1% [41]. However, in [41] we identified strong dependence of estimation accuracy to the number of measurement points, as high number is required for accurate estimation of characteristic frequency. In the rest of this paper we will present approach to reduce need for high number of measurement points but to keep the same estimation accuracy without significant increase in algorithm complexity as well.

2.2 Influence of Uncertainty in Characteristic Frequency on Estimated Values of Model Parameters

If instead of exact value of characteristic angular frequency for the given 2R-1C model, value $\hat{p} = \mu \cdot p$ is estimated from measured data (μ is real number) relative errors for estimated values $\hat{K}(\omega_i)$ and $\hat{z}(\omega_i)$ can be calculated:

$$\delta z(\omega_i) = \frac{\hat{z}(\mu \cdot p, \omega_i) - z}{z}$$

$$= \frac{(1-\mu)\cdot p\cdot \omega_i \cdot (X^2(\omega_i)+R^2(\omega_i))}{(\omega_i\cdot R(\omega_i)+\mu\cdot p\cdot X(\omega_i))\cdot(\omega_i\cdot X(\omega_i)-p\cdot R(\omega_i))} \tag{16}$$

and

$$\delta K(\omega_i) = \frac{\hat{K}(\mu\cdot p,\omega_i)-K}{K} = \frac{p\cdot(\mu-1)\cdot X(\omega_i)}{p\cdot X(\omega_i)+\omega_i\cdot R(\omega_i)}. \tag{17}$$

Calculations of relative errors for estimated $\hat{R}_1$, $\hat{R}_2$ and $\hat{C}_2$ can be done in similar way, but because estimated values of model parameters are means of (13)-(15), thus they are frequency independent, it is more useful to calculate relative errors as:

$$\delta\hat{R}_1 = \frac{\frac{1}{N}\sum_{i=1}^{N}\hat{R}_1(\omega_i)-R_1}{R_1} = \frac{\hat{R}_1-R_1}{R_1} \tag{18}$$

$$\delta\hat{R}_2 = \frac{\frac{1}{N}\sum_{i=1}^{N}\hat{R}_2(\omega_i)-R_2}{R_2} = \frac{\hat{R}_2-R_2}{R_2} \tag{19}$$

$$\delta\hat{C}_2 = \frac{\frac{1}{N}\sum_{i=1}^{N}\hat{C}_2(\omega_i)-C_2}{C_2} = \frac{\hat{C}_2-C_2}{C_2} \tag{20}$$

where R_1, R_2 and C_2 are actual values of model parameters, while $\hat{R}_1(\omega_i)$, $\hat{R}_2(\omega_i)$ and $\hat{C}_2(\omega_i)$ are defined with (13), (14) and (15), respectively.

2.3 Influence of Number of Measurement Frequencies on Estimation of Characteristic Frequency

Number of measurement frequencies N is usually limited by complexity of used measurement and data acquisition units, and their capabilities to handle a wide frequency range, small frequency step and large amount of data. However, in many applications large number of measurement frequencies is required to allow identification and analysis of involved processes. Thus, optimization of number of measurement points is very common and non-easy task to accomplish.

It is more convenient to use f [Hz] instead of ω [rad/s] for specifications regarding frequency range and characteristic frequency of impedance. Because of that, we will define frequency range as ($f_{\min}$, $f_{\max}$). Number of measurement frequencies in analyzed frequency range defines the frequency step Δf as:

$$\Delta f = \frac{f_{\max}-f_{\min}}{N}. \tag{21}$$

In Fig. 3 locations of the few measurement points on the frequency axis with typical curve $X(f)$ of 2R-1C model are given. If characteristic frequency f_c is located between two measurement points (f_i, f_{i+1}) the biggest possible absolute error in characteristic frequency estimation is $\hat{f}_c - f_c = 0.5\Delta f$.

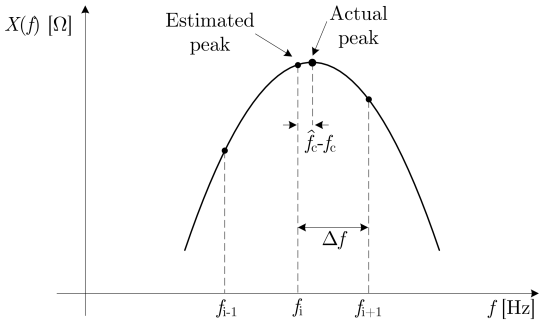

Fig. 3 Error in characteristic frequency estimation due to limited number of the measurement frequencies.

If maximum acceptable relative error in characteristic frequency estimation is pre-defined with given requirement δf_c, and because the biggest absolute error in characteristic frequency estimation is $\hat{f}_c - f_c = 0.5\Delta f$, it is possible to define required frequency step or number of measurement frequencies in the analyzed frequency range as threshold to satisfy that requirement. The highest number of measurement frequencies is required if characteristic frequency is equal to the lower frequency limit ($f_c = f_{\min}$):

$$N = \frac{f_{\max} - f_{\min}}{2 \cdot f_c \cdot \delta f_c} \tag{22}$$

which requires the smallest frequency step

$$\Delta f = 2 \cdot \delta f_c \cdot f_c. \tag{23}$$

We defined threshold N or Δf to ensure that relative error is smaller than defined δf_c. However, it is possible for some lower values of N to have smaller error if $(f_{\min} + h\Delta f) \approx f_c$ where h is integer. For example, if analyzed frequency range is from 10 kHz to 100 kHz and if characteristic frequency is f_c=50 kHz, then N=10, which corresponding to frequency step of Δf=10 kHz, will make smaller error in characteristic frequency estimation than N=15 which corresponding to frequency step of Δf=6 kHz. However, such approach is not reliable and it is usually very hard to predict optimal value for N to minimize estimation error.

2.4 Solving a Set of Nonlinear Equations Using Quadratic Interpolation for More Accurate Estimation of Characteristic Frequency

Estimation accuracy of characteristic frequency based on finding the maximum magnitude (peak of the curve) of the measured imaginary part can be affected by the limited number of measurement frequencies or by noise. In this paper we will not analyze noise influence because we will consider case that signal was filtered prior to the parameter estimation. A comprehensive analysis of

noise influence and design of appropriate filter will be the subject of our future work.

Limited number of measurement frequencies leads to possibility that point equal to characteristic frequency can be missed in frequency sweep, as it is shown in Fig. 3. In order to increase accuracy of characteristic frequency estimation it is required to have more accurate estimated peak of imaginary part of impedance. Our approach is to use three-point quadratic interpolation of impedance measurement values of imaginary part around estimated peak β as shown in Fig. 4:

$$X(\omega_{\text{n-1}}) = \alpha \tag{24}$$

$$X(\omega_{\text{n}}) = \beta \tag{25}$$

$$X(\omega_{\text{n+1}}) = \gamma. \tag{26}$$

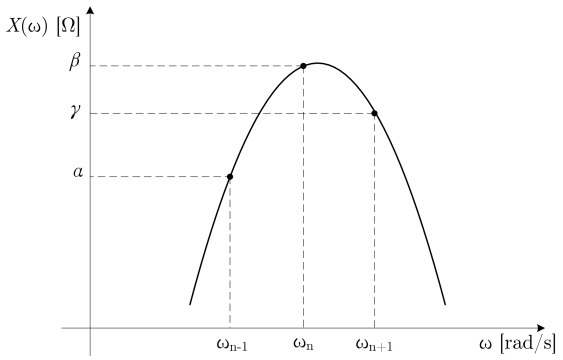

Fig. 4 Values of imaginary part of impedance around peak β.

Solving the set of three nonlinear equations (24)-(26) using quadratic interpolation

$$a\omega^2 + b\omega + c = X(\omega) \tag{27}$$

gives following solution:

$$a = -\frac{(\alpha-\beta)\cdot\omega_{\text{n+1}} - (\alpha-\gamma)\cdot\omega_{\text{n}} + (\beta-\gamma)\cdot\omega_{\text{n-1}}}{(\omega_{\text{n-1}}-\omega_{\text{n}})\cdot(\omega_{\text{n-1}}-\omega_{\text{n+1}})\cdot(\omega_{\text{n}}-\omega_{\text{n+1}})} \tag{28}$$

$$b = -\frac{\alpha\cdot(\omega_{\text{n}}^2-\omega_{\text{n+1}}^2) - \beta\cdot(\omega_{\text{n-1}}^2-\omega_{\text{n+1}}^2)}{(\omega_{\text{n-1}}-\omega_{\text{n}})\cdot(\omega_{\text{n-1}}-\omega_{\text{n+1}})\cdot(w_{\text{n}}-\omega_{\text{n+1}})}$$
$$-\frac{\gamma\cdot(\omega_{\text{n-1}}^2-\omega_{\text{n}}^2)}{(\omega_{\text{n-1}}-\omega_{\text{n}})\cdot(\omega_{\text{n-1}}-\omega_{\text{n+1}})\cdot(w_{\text{n}}-\omega_{\text{n+1}})} \tag{29}$$

$$c = \frac{(\alpha-\gamma)\cdot\omega_{\text{n-1}}\cdot\omega_{\text{n}}}{(\omega_{\text{n-1}}-\omega_{\text{n}})\cdot(\omega_{\text{n-1}}-\omega_{\text{n+1}})} - \frac{\alpha\cdot\omega_{\text{n}}-\beta\cdot\omega_{\text{n-1}}}{\omega_{\text{n-1}}-\omega_{\text{n}}}$$
$$-\frac{(\beta-\gamma)\cdot\omega_{\text{n-1}}\cdot\omega_{\text{n}}}{(\omega_{\text{n-1}}-\omega_{\text{n}})\cdot(\omega_{\text{n}}-\omega_{\text{n+1}})}. \tag{30}$$

With calculated values a, b and c it is possible to estimate corrected peak of imaginary part of impedance, and therefore corrected characteristic angular frequency of the 2R-1C model:

$$\hat{p}_{\mathrm{corr}} = -\frac{b}{2a}. \tag{31}$$

Our approach is to use $\hat{p}_{\mathrm{corr}}$, (11) and (12) for the 2R-1C model parameters estimation with (13), (14) and (15).

3 EXPERIMENTAL RESULTS

3.1 Simulation

3.1.1 Data Generation

As a part of validation process of the non-iterative method described in Section 2, we analyzed parameter estimation of the 2R-1C models with numerically calculated (simulated) impedance data. Reference values were chosen as R_1=1 kΩ, R_2=470 Ω and C_2 = 4.7 nF as standard and widely available as real components for latter hardware-based experiment. Characteristic angular frequency ω_{c} of analyzed 2R-1C model is calculated using (9) for given reference values as ω_{c}=144738.750 rad/s while corresponding characteristic frequency is f_{c}=23035.887 Hz. Complex impedance data was calculated using (1) in frequency range from 5 kHz to 100 kHz, which is common for low-cost and widely used microcontroller-based impedance meters [38].

3.1.2 Influence of Uncertainty in Characteristic Frequency on Estimated Values of Model Parameters

Instead of use of the actual values of characteristic frequency, we varied values of μ from ±0.01, ±0.02, ±0.05 to ±0.1. Thus, we introduced relative errors ($\delta f_{\mathrm{c}}(\%)$) in characteristic frequencies estimation of ±1%, ±2%, ±5% and ±10%, respectively. We wanted additionally to analyze if sign in relative error in characteristic frequency estimation makes some difference on estimated values of model parameters. Number of measurement frequencies (10, 100 and 1000) was chosen arbitrarily to adequately cover analyzed frequency range. Estimated values of model parameters using approach without quadratic interpolation are presented in Table 1.

Table 1 Relative Errors for Estimated Values of Model Parameters for Different δf_c[%].

N	δf_c[%]	δR_1[%]	δR_2[%]	δC_2[%]
10	10	-4.338	-6.853	-4.130
100	10	-4.475	-6.202	-4.253
1000	10	-4.488	-6.141	-4.265
10	5	-2.272	-3.486	-2.151
100	5	-2.344	-3.134	-2.217
1000	5	-2.351	-3.101	-2.223
10	2	-0.936	-1.409	-0.881
100	2	-0.965	-1.262	-0.910
1000	2	-0.968	-1.248	-0.913
10	1	-0.473	-0.707	-0.445
100	1	-0.487	-0.632	-0.459
1000	1	-0.489	-0.625	-0.460
10	-1	0.482	0.712	0.452
100	-1	0.498	0.635	0.467
1000	-1	0.499	0.627	0.468
10	-2	0.974	1.429	0.913
100	-2	1.005	1.272	0.942
1000	-2	1.008	1.258	0.945
10	-5	2.512	3.612	2.342
100	-5	2.591	3.199	2.418
1000	-5	2.598	3.161	2.425
10	-10	5.303	7.359	4.898
100	-10	5.469	6.462	5.060
1000	-10	5.485	6.379	5.075

As it can be seen from Table 1, relative errors in estimation of parameters were lower than $\pm 1\%$ if δf_c is $\pm 1\%$. Moreover, if $\mu < 1$ relative errors were positive, and if $\mu > 1$ relative errors were negative. Number of measurement frequencies did not make significant difference on estimated values, thus number of measurement frequencies is only important for estimation of characteristic frequency. Relative errors lower or up to 1% in estimation of values of model parameters are usually acceptable in many practical cases, and we will consider that case in the rest of the paper. Thus, our target was estimation of characteristic frequency with error lower than 1%.

3.1.3 Influence of Number of Measurement Frequencies on Estimation of Characteristic Frequency

If analyzed frequency range is from 5 kHz to 100 kHz and defined $\delta f_c = 0.01$ (1% error), the highest number of measurement frequencies is required if f_c=5 kHz. According to (22) required frequency step is 100 Hz or N=950. Using approach without quadratic interpolation estimated value of characteristic frequency of analyzed the 2R-1C model when N=950 is $\hat{f}_c$=23018.967 Hz. Thus, characteristic frequency is estimated with relative error -0.073%. Estimated value for characteristic angular frequency was used with described non-iterative method for parameter estimation of analyzed 2R-1C model with-

out quadratic interpolation. As it was expected, values of model parameters $\hat{R}_1$=1000.363 Ω, $\hat{R}_2$= 470.216 Ω, $\hat{C}_2$=4.702 nF were estimated with very small relative errors: δR_1= 0.036%, δR_2= 0.046% and δC_2= 0.034%.

However, relative high number of measurement points of 950 is not suitable for low-cost impedance meters because of requirement of advanced data acquisition unit as well as high processing time. Moreover, in many practical applications [5], characteristic frequency is usually a few tens of kHz, which can significantly reduce required number of measurement frequencies. For example, studies of bioimpedance showed that mean values of characteristic frequencies are 80.1 kHz and 57 kHz for women and men, respectively [11, 21, 37, 47]. Median values of characteristic frequencies are 32 kHz for males and 35 kHz for females [46]. Thus, previous knowledge of analyzed system is very useful in reduction of required number of measurement points. Moreover, approximate location of characteristic frequency can be found with initial impedance measurement (screening) with just few measurement points. For example, if minimum possible f_c is 20 kHz, then according to (22) N=238 should ensure less than 1% error in characteristic frequency estimation.

Estimated value of characteristic frequency of analyzed 2R-1C model when N=238 is $\hat{f}_c$=23035.889 Hz. Thus, characteristic frequency is estimated with error 0.009%. Estimated value for characteristic angular frequency were used with described non-iterative method for parameter estimation of analyzed 2R-1C model without quadratic interpolation. As it was expected, values of model parameters $\hat{R}_1$=999.955 Ω, $\hat{R}_2$=469.973 Ω, $\hat{C}_2$=4.700 nF were estimated with very small relative errors: δR_1= -0.004%, δR_2= 0.040% and δC_2= 0.004%.

3.1.4 More Accurate Characteristic Frequency Estimation of 2R-1C Model Using Quadratic Interpolation

Our approach, described in Section 2.4, is to reduce number of measurement points but to keep the relative high accuracy in estimation of values of model parameters using quadratic interpolation of measurement values around peak of imaginary part of impedance. We started with N=238, and then N was decreasing to 3 as minimum number of measurement points to implement quadratic interpolation. Parameter $\hat{p}$ was estimated using (28)-(30) and (31), while δf_c was monitored. Our tests showed that, in case of the analyzed 2R-1C model, it was possible to reduce N to 29 as threshold to have relative error in characteristic frequency estimation lower than 1%, as it is shown in Fig. 5. As it was expected, without quadratic interpolation it was required much higher number of measurement frequencies (N=173). Additionally, for N=29 relative error in characteristic frequency estimation without quadratic interpolation was 4.652%.

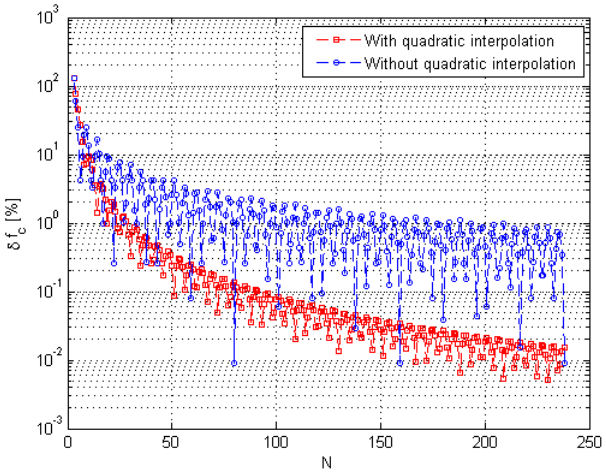

Fig. 5 Comparison of relative errors in characteristic frequency estimation.

Methods with and without quadratic interpolation were compared regarding relative errors in estimated values of model parameters as well. Relative errors in parameter estimation of model values (R_1, R_2 and C_2) with and without quadratic interpolation for different numbers of measurement frequencies are shown in Fig. 6-8, respectively.

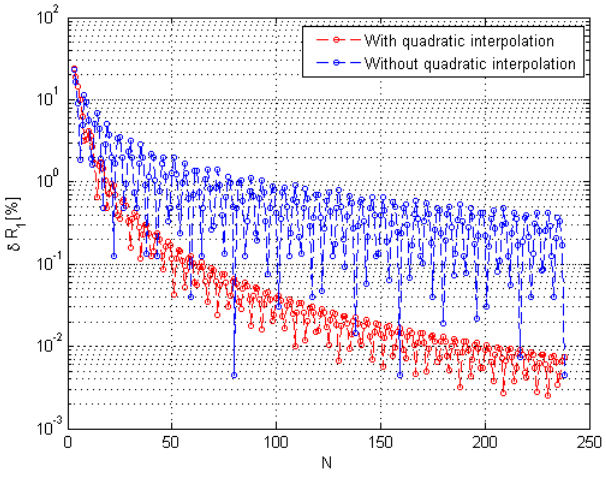

Fig. 6 Comparison of relative errors in estimation of R_1.

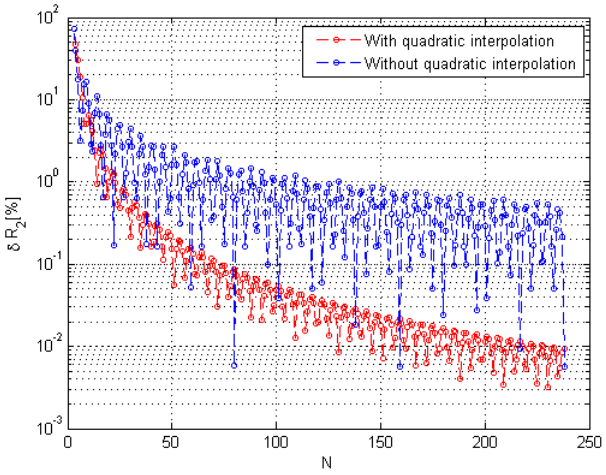

Fig. 7 Comparison of relative errors in estimation of R_2.

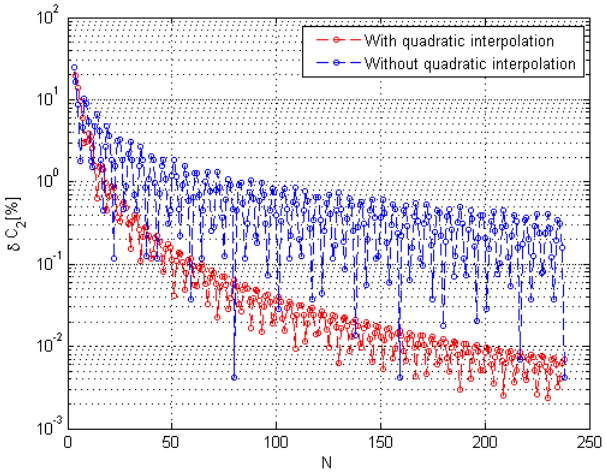

Fig. 8 Comparison of relative errors in estimation of C_2.

As it can be seen from Fig. 6-8, with quadratic interpolation it was possible to have 1% relative error in parameter estimation with 80% reduced number of measurement points (N=23) in comparison with approach without quadratic interpolation (N=115).

3.1.5 Parameter Estimation of the 2R-1C Model from Electrical Bioimpedance Data

To obtain more quantitative characterization of the proposed method we have performed parameter estimation of 2R-1C models which reference values were estimated from six common electrical bioimpedance (EBI) measurements: Total Body Composition (TBC), Respiration Rate (RR), Trunk-Trunk (TT), Leg-Leg (LL), Lung Composition (LC) and Arm-Arm (AA) [13]. Reference values for model parameters as well as characteristic frequencies are shown in Table 2.

Table 2 Reference values for 2R-1C models parameters [13].

EBI	R_1 [Ω]	R_2 [Ω]	C_2 [nF]	f_c [Hz]
TBC	917.5	629.0	3.42	30091.52
RR	58.5	23.9	75.7	25515.09
TT	99.0	42.3	44.0	25599.14
LL	510.0	450	6.55	25310.90
LC	81.46	19.64	47.7	33002.79
AA	364.6	379.0	6.2	34521.45

Values from Table 2 were used to calculate reference impedance data in frequency range from 5 kHz to 100 kHz. Experiment was started with N=950 and then number of measurement frequencies was decreased with aim to compare threshold required to have relative errors lower than 1% in estimation of all three model parameters. Both approaches, with and without quadratic interpolation, were used on the same dataset and in Table 3 obtained results are presented.

Table 3 Comparison of the minimum number of measurement points required for relative errors lower than 1%.

EBI	Without quadratic interpolation	With quadratic interpolation	Reduction of measurement points [%]
TBC	91	17	81.319
RR	148	25	83.108
TT	138	25	81.834
LL	112	21	81.250
LC	231	29	87.446
AA	84	15	82.143

As it can be seen from Table 3, approach with quadratic interpolation required more than 80% less measurement points to achieve estimation error for all three model parameters lower than 1%.

Moreover, we have compared execution time of approaches with and without quadratic interpolation. Additionally we have compared execution times

of approach with quadratic interpolation and CNLS for the same number of measurement points N. Our test platform was MATLAB R2013b installed on Lenovo notebook with i5-4300M CPU at 2.60 GHz and 64-bit Windows 7 operating system. CNLS estimation was performed with MATLAB's function *lsqcurvefit* (Levenberg-Marquardt algorithm). Maximum number of function evaluations and maximum number of iterations were set to 10^3, while termination tolerance on the function value and termination tolerance on estimated vector were set to 10^{-4}. To increase the speed of estimation, analytical expressions for Jacobian was supplied to the solver. Measuring performances using stopwatch timer (*tic* and *toc* MATLAB commands), as shown in Table 4, we determined that the approach with quadratic interpolation requires slightly higher processing time. However, it requires significantly lower number of measurement points for 1% error which can be a huge advantage if low-cost microcontroller-based devices are used. Moreover, in conducted experiment approach with quadratic interpolation was 30-45 times faster than CNLS, but CNLS approach estimated values of model parameters with error lower than 0.005%.

Table 4 Comparison of execution times.

		TBC	RR	TT	LL	LC	AA
Without quadratic	N	91	148	138	112	231	84
interpolation	t [ms]	4.561	5.067	5.865	3.386	3.298	3.871
With quadratic	N	17	25	25	21	29	15
interpolation	t [ms]	5.060	5.949	7.037	4.480	4.085	3.895
CNLS	N	17	25	25	21	29	15
	t [ms]	180.621	190.501	190.925	193.935	179.834	186.247

3.2 Hardware-Based Experiment

The AD5933-based impedance measurement system (Fig. 9) reported earlier [42] was used for impedance measurement of the analyzed 2R-1C model. Device is based on 8-bit ATmega128 microcontroller and integrated circuit AD5933. Communication between microcontroller and the AD5933 (device initialization, definition of measurement details and collecting measurement data) is via I2C protocol. With developed device it is possible to perform frequency sweep impedance measurement in frequency range from 5 kHz to 100 kHz with maximum 511 points and frequency step as low as 0.1 Hz.

Accuracy tests of developed impedance measurement device have been performed with series and parallel RC networks with values for R and C chosen to ensure wide range of impedance magnitude and phase angle change. Obtained results were compared with reference measurement results obtained with Agilent 4263B LCR meter and Impedance/Gain-Phase Analyzer 4194A from Hewlett Packard. For impedance magnitude in range from 100 Ω to 100 kΩ maximum system error for magnitude and phase angle measurements was less than 3% and 2.5° in complete frequency range, respectively [39, 40].

Towards practical applications for real-time impedance measurement and parameters estimation with developed device, investigation how long is required to collect impedance data for one measurement point is required. The theoretical sample time for a single measurement with the AD5933 is sum of [14]:

- time required for the AD5933 to estimate the impedance values, and it is approximately 1 ms for a commonly used system clock of 16 MHz,
- total time to perform all the I2C protocol instructions,
- settling cycles time, which can be calculated by the multiplication of the total number of the settling cycles and the period of the excitation signal.

For the I2C frequency of 400 kHz, one settling cycle and exication frequency of 50 kHz, the theoretical impedance sampling time is 1.895 ms, while experimentally obtained time to perform all operations required for one measurement at 50 kHz is around 1.7910 ms [14]. For excitation frequency of 100 kHz it is around 1.7911 ms [14]. Experimentally obtained values are mean for 100 repeated measurements.

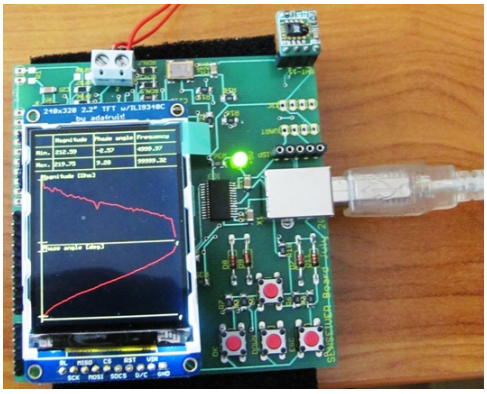

Fig. 9 The AD5933-based impedance measurement device.

The 2R-1C model has been made with the real components chosen with nominal values as it was used in simulation part: R_1=1000 Ω±5%, R_2=470 Ω±5% and C_2=4.7 nF±5%. With these values nominal characteristic frequency can be calculated as 23035.887 Hz. Using the AD5933-based measurement device impedance measurement of used components in frequency range from 5 kHz to 100 kHz was performed. Obtained results (mean values ± standard deviation) are: R_1=983.37 Ω±0.67 Ω, R_2=463.49 Ω±1.22 Ω, and C_2=4.55 nF±0.06 nF. Using mean values characteristic frequency can be calculated as 24175.876 Hz. As it can be seen there is a slight difference in comparison with nominal values of model parameters and characteristic frequency.

Impedance measurement of the 2R-1C model was performed in frequency range from 5 kHz to 100 kHz in 29 frequency points, because in simulation

part $N = 29$ was obtained as a threshold for 1% relative error in characteristic frequency estimation using quadratic interpolation.

We have compared approaches with and without quadratic interpolation in microcontroller-based implementation. Our test platform was Arduino Uno board. Arduino Uno is based on ATmega328P microcontroller with 2 KB SRAM, 16 MHz clock speed and in total 32 KB flash memory. Estimated values of characteristic frequency, mean values of model parameters $\hat{R}_1, \hat{R}_2$, and $\hat{C}_2$, and standard deviations σR_1, σR_2 and σC_2 from measured data with and without quadratic interpolation are shown in Table 5.

Table 5 Estimated values of characteristic frequency and model parameters for N=29.

	$\hat{f}_c$[Hz]	$\hat{R}_1[\Omega]\pm\sigma R_1[\Omega]$	$\hat{R}_2[\Omega]\pm\sigma R_2[\Omega]$	$\hat{C}_2$[nF]$\pm\sigma C_2$[nF]
Nominal values	23035.887	1000±5%	470±5%	4.7±5%
Measured	24175.876	983.37±0.67	463.49±1.22	4.550±0.06
Estimated without quadratic interpolation	23352.000	955.653±13.563	467.185±10.916	4.412±0.018
Estimated with quadratic interpolation	24409.671	972.629±8.290	479.621±5.647	4.490±0.04

As it is shown in Table 5, standard deviations of mean values $\hat{R}_1, \hat{R}_2$, and $\hat{C}_2$ estimated without quadratic interpolation are 1.419%, 2.337% and 0.406%, respectively. With quadratic interpolation these values are 0.852%, 1.167% and 0.913%. Additionally, we have explored frequency dependences of estimated values of model parameters. Estimated values of $\hat{R}_1$, $\hat{R}_2$, and $\hat{C}_2$ at different frequencies are shown in Fig. 10-Fig. 12. As it was expected from Table 5, values estimated with quadratic interpolation have lower frequency dependence.

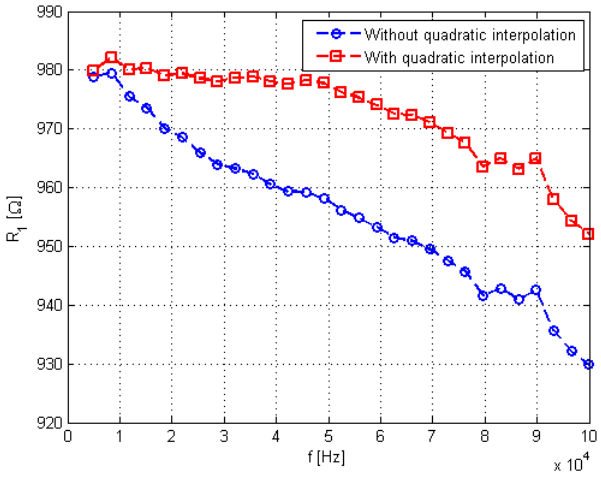

Fig. 10 Estimated values of $\hat{R}_1$ at different frequencies.

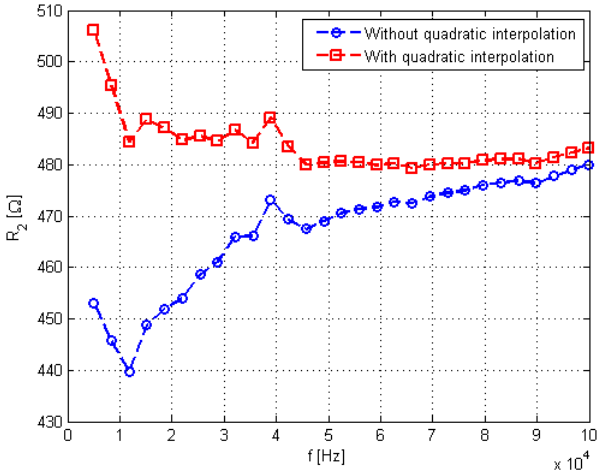

Fig. 11 Estimated values of $\hat{R}_2$ at different frequencies.

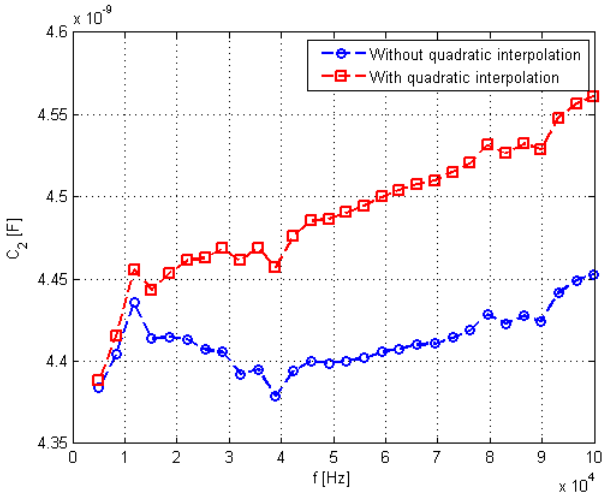

Fig. 12 Estimated values of $\hat{C}_2$ at different frequencies.

Values estimated with and without quadratic interpolation are used to calculate impedance of the 2R-1C model using (4) in frequency range from 5 kHz to 100 kHz in 29 points. Comparison of calculated values with measured data is shown in Fig. 13.

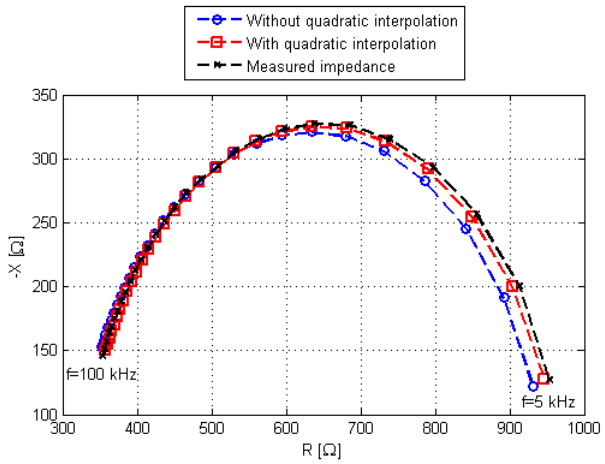

Fig. 13 Comparison of measured impedance and impedance calculated with estimated values of model parameters.

Because of tolerance of nominal values and frequency dependent characteristics of used components, as well as measurement noise there is a lack of

actual reference values for model parameters. Because of that, we choose to compare measured impedance and impedance calculated with estimated values of model parameters. Relative errors ($\delta R(\omega)[\%]$ and ($\delta X(\omega)[\%]$)) for real and imaginary part of measured and calculated impedance are shown in Fig. 14 and Fig. 15, respectively.

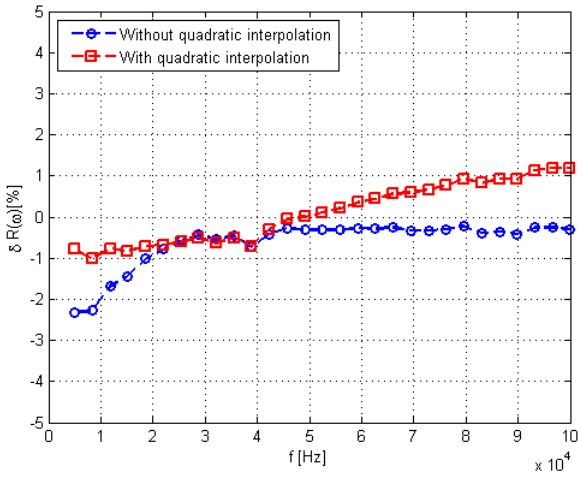

Fig. 14 Comparison of relative errors for real part of impedance.

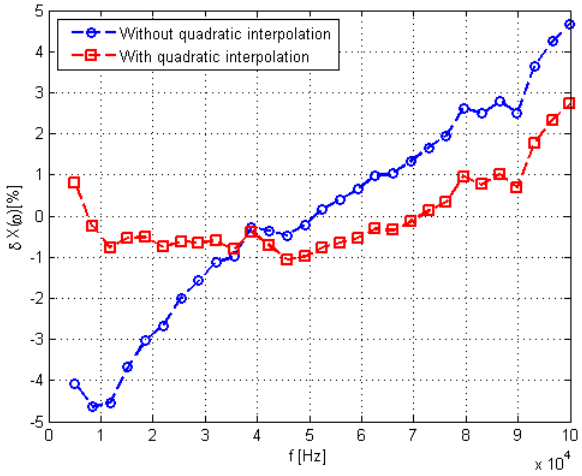

Fig. 15 Comparison of relative errors for imaginary part of impedance.

As it can be seen from Fig. 14 and Fig. 15, maximum differences between measured and impedance calculated with quadratic interpolation are smaller for real part of impedance ($\pm 1.197\% < \pm 2.328\%$) as well as for imaginary part of impedance ($\pm 2.722\% < \pm 4.667\%$).

Additionally we have compared Root Mean Square Errors (RMSE) for measured ($\mathbf{R}_{\text{meas}}$ and $\mathbf{X}_{\text{meas}}$) and impedance ($\mathbf{R}_{\text{calc}}$ and $\mathbf{X}_{\text{calc}}$) calculated with values of model parameters estimated without and with quadratic interpolation, using equations for real

$$\text{RMSE}_R = \sqrt{\frac{\sum_{i=1}^{N}(R_{\text{calc}}(\omega_i) - R_{\text{meas}}(\omega_i))^2}{N}} \tag{32}$$

and imaginary part of impedance

$$\text{RMSE}_X = \sqrt{\frac{\sum_{i=1}^{N}(X_{\text{calc}}(\omega_i) - X_{\text{meas}}(\omega_i))^2}{N}}. \tag{33}$$

Obtained values are shown in Table 6. As it can be seen, RMSE for calculated impedance with quadratic interpolation are smaller for 42.828% (real part) and 51.515% (imaginary part) in comparison for estimation without quadratic interpolation.

Table 6 Comparison of RMSE for real and imaginary part of impedance.

	Without quadratic interpolation	With quadratic interpolation
RMSE_R	7.015 Ω	4.011 Ω
RMSE_X	5.483 Ω	1.944 Ω

Measuring performances using Arduino stopwatch timer (function *micros*()) we determined that approach without quadratic interpolation estimated values in 8.592 ms, while for approach with quadratic interpolation it was required 9.168 ms. Moreover, approach with quadratic interpolation required 6306 bytes of flash memory and 1396 bytes of RAM, while approach without quadratic interpolation required 5060 bytes of flash memory and 1364 bytes of RAM as shown in Table 7.

Table 7 Performance comparison of approaches implemented on ATmega328P microcontroller.

	Without quadratic interpolation	With quadratic interpolation
Execution time [ms]	8.592	9.168
Flash memory [bytes]	5060	6306
RAM [bytes]	1364	1396

Even we can recognize that approach with quadratic interpolation requires 6.7% higher execution time, 24% more flash memory and 2.4% more RAM it is still acceptable for practical use with low-cost microcontroller based devices.

4 CONCLUSION

In this paper the method for non-iterative parameter estimation of the 2R-1C model suitable for low-cost embedded hardware is presented. Approach is based on use of quadratic interpolation for estimation of characteristic frequency while the model parameters are calculated on provided set of analytical expressions. Compared to the estimation approach without quadratic interpolation, with described method it was possible to have the same relative error in parameter estimation (lower than 1%) with 80% lower number of measurement points.

Our hardware-based experiments showed suitability of proposed method for low-cost microcontroller-based devices with limited resources regarding power consumption, computation complexity and RAM usage. Obtaining results are promising for applications where portable operation is needed as it eliminates need for complex data postprocessing.

As a future work we are directed towards integration of AD5933-based impedance measurement system with presented non-iterative approach in compact unit for *in-situ* parameter estimation of sensors or bioimpedance analysis. Moreover, such integration requires design of appropriate filter for denoising measurement impedance data which will be also part of our future work in this field.

Acknowledgements The research was supported by the Ministry of Science and Technology of the Republic of Srpska under contract 19/6-020/961-37/15, and by the EU's H2020 MSCA project no. 690876.

5 Appendix

5.1 Code for Arduino implementation of approach without quadratic interpolation.

```
1 float freq[29]={5000, 8392, 11784, 15176, 18568, 21960,
    25352, 28744, 32136, 35528, 38920, 42312, 45704,
    49096, 52488, 55880, 59272, 62664, 66056, 69448,
    72840, 76232, 79624, 83016, 86408, 89800, 93192,
    96584, 99976};
2 float real[29]={953.83, 913.05, 856.03, 797.76, 739.06,
    685.83, 638.43, 597.17, 563.11, 532.74, 508.71,
    485.33, 466.04, 450.31, 436.57, 424.68, 414.17,
    405.25, 397.23, 390.55, 384.4, 378.86, 373.73,
    369.97, 365.97, 362.66, 358.95, 356.06, 353.64};
3 float imag[29]={-127.03, -200.81, -257.01, -293.67,
    -315.51, -326.35, -327.49, -323.5, -315.68, -306.52,
     -294.35, -284.0, -273.58, -262.24, -250.99,
    -240.52, -230.58, -221.0, -212.51, -204.05, -196.0,
```

```
    -188.53, -180.81, -174.94, -168.7, -163.73, -156.88,
     -151.2, -146.11};
float w[29];
char i = 0;
float maxImag = 0.0;
char index = 0;
float z_pom_1[29], K[29], Re_est[29], Ri_est[29], Cm_est
    [29];
float p_e1 = 0;
float Re_est_alg1=0, Ri_est_alg1=0, Cm_est_alg1=0;
float sum1 = 0, sum2 = 0, sum3 = 0;
unsigned long duration_alg1=0;

void setup()
{
  Serial.begin(9600);
  while (!Serial)
  {
    ;
  }
  for(i=0;i<29;i++)
  {
    w[i] = 2.0*22.0*freq[i]/7.0;
  }

  duration_alg1 = micros();
  maxImag=abs(imag[0]);
  index = 0;
  for(i=1; i<29; i++)
  if (abs(imag[i])>=maxImag)
  {
    maxImag = abs(imag[i]);
    index = i;
  }
  p_e1 = freq[index];
  p_e1 = 2.0*22.0*p_e1/7.0;

  sum1 = 0;
  sum2 = 0;
  sum3 = 0;

for(i=0;i<29;i++)
{
  z_pom_1[i] = -(imag[i]*w[i]*w[i] - real[i]*p_e1*w[i])
      /(imag[i]*p_e1 + real[i]*w[i]);
  K[i]=(real[i]*w[i]+imag[i]*p_e1)/(w[i]);
```

```
  Re_est[i] = z_pom_1[i]*K[i]/p_e1;
  Ri_est[i] = K[i]* Re_est[i]/(Re_est[i]-K[i]);
  Cm_est[i] = (Re_est[i] - K[i])/(z_pom_1[i]*K[i]*Re_est
      [i]);
  sum1 +=  Re_est[i] ;
  sum2 +=  Ri_est[i] ;
  sum3 +=  Cm_est[i] ;
}

  Re_est_alg1 = sum1 / 29.0 ;
  Ri_est_alg1 = sum2 / 29.0 ;
  Cm_est_alg1 = sum3 / 29.0 ;

  duration_alg1 = micros() - duration_alg1;
  Serial.print("Without␣quadratic␣interpolation:␣");
  Serial.print(duration_alg1);
  Serial.println("␣us");
  Serial.print("R1_alg1=␣");
  Serial.println(Re_est_alg1);
  Serial.print("R2_alg1=␣");
  Serial.println(Ri_est_alg1);
  Serial.print("C2_alg1=␣");
  Serial.print(Cm_est_alg1*1e9);
  Serial.println("␣nF");
  Serial.print("Fc_alg1=␣");
  Serial.println(p_e1/(2.0*22.0/7.0));
}

void loop()
{
}
```

5.2 Code for Arduino implementation of approach with quadratic interpolation.

```
float freq[29]={5000, 8392, 11784, 15176, 18568, 21960,
    25352, 28744, 32136, 35528, 38920, 42312, 45704,
    49096, 52488, 55880, 59272, 62664, 66056, 69448,
    72840, 76232, 79624, 83016, 86408, 89800, 93192,
    96584, 99976};
float real[29]={953.83, 913.05, 856.03, 797.76, 739.06,
    685.83, 638.43, 597.17, 563.11, 532.74, 508.71,
    485.33, 466.04, 450.31, 436.57, 424.68, 414.17,
    405.25, 397.23, 390.55, 384.4, 378.86, 373.73,
    369.97, 365.97, 362.66, 358.95, 356.06, 353.64};
```

```
3 float imag[29]={-127.03, -200.81, -257.01, -293.67,
    -315.51, -326.35, -327.49, -323.5, -315.68, -306.52,
     -294.35, -284, -273.58, -262.24, -250.99, -240.52,
    -230.58, -221, -212.51, -204.05, -196, -188.53,
    -180.81, -174.94, -168.7, -163.73, -156.88, -151.2,
    -146.11};
4 float w[29];
5 char i = 0;
6 float maxImag = 0.0;
7 char index = 0;
8 float z_pom_1[29], K[29], Re_est[29], Ri_est[29], Cm_est
    [29];
9 float sum1 = 0.0, sum2 = 0.0, sum3 = 0.0;
10 float alpha = 0.0, beta = 0.0, gamma = 0.0, w1 = 0.0, w2
     = 0.0, w3 = 0.0;
11 float a = 0.0, b = 0.0, c = 0.0, vertex = 0.0, fc_e2 =
    0.0;
12 float p_interpolation = 0;
13 float Re_est_alg2=0.0, Ri_est_alg2=0.0, Cm_est_alg2=0.0;
14
15 unsigned long duration_alg2=0;
16
17 void setup()
18 {
19   Serial.begin(9600);
20   while (!Serial)
21   {
22     ;
23   }
24   for(i=0;i<29;i++)
25   {
26     w[i] = 2.0*22.0*freq[i]/7.0;
27   }
28
29   duration_alg2 = micros();
30   maxImag=abs(imag[0]);
31   index = 0;
32   for(i=1; i<29; i++)
33   if (abs(imag[i])>=maxImag)
34   {
35     maxImag = abs(imag[i]);
36     index = i;
37   }
38   alpha=abs(imag[index-1]);
39   beta=abs(imag[index]);
40   gamma=abs(imag[index+1]);
```

```
41  w1=w[index-1];
42  w2= w[index];
43  w3= w[index+1];
44
45  a = (alpha*w2 - alpha*w3 - beta*w1 + beta*w3 + gamma*
        w1 - gamma*w2)/((w1 - w2)*(w1*w2 - w1*w3 - w2*w3 +
         w3*w3));
46  b = -(alpha*w2*w2 - alpha*w3*w3 - beta*w1*w1 + beta*w3
        *w3 + gamma*w1*w1 - gamma*w2*w2)/((w1 - w2)*(w1*w2
         - w1*w3 - w2*w3 + w3*w3));
47  c = -(- gamma*w1*w1*w2 + beta*w1*w1*w3 + gamma*w1*w2*
        w2 - beta*w1*w3*w3 - alpha*w2*w2*w3 + alpha*w2*w3*
        w3)/((w1 - w2)*(w1*w2 - w1*w3 - w2*w3 + w3*w3));
48  p_interpolation = -b/(2*a);
49  sum1=0.0;
50  sum2=0.0;
51  sum3=0.0;
52
53  for (i = 0 ; i < 29; i++)
54  {
55   z_pom_1[i] = -(imag[i]*w[i]*w[i] - real[i]*
        p_interpolation*w[i])/(imag[i]*p_interpolation +
        real[i]*w[i]);
56   K[i]=(real[i]*w[i]+imag[i]*p_interpolation)/(w[i]);
57   Re_est[i] = z_pom_1[i]*K[i]/p_interpolation;
58   Ri_est[i] = K[i]* Re_est[i]/(Re_est[i]-K[i]);
59   Cm_est[i] = (Re_est[i] - K[i])/(z_pom_1[i]*K[i]*
        Re_est[i]);
60   sum1 +=  Re_est[i] ;
61   sum2 +=  Ri_est[i] ;
62   sum3 +=  Cm_est[i] ;
63  }
64  Re_est_alg2 = (float)sum1 / 29.0 ;
65  Ri_est_alg2 = (float)sum2 / 29.0 ;
66  Cm_est_alg2 = (float)sum3 / 29.0 ;
67
68  duration_alg2 = micros() - duration_alg2;
69
70  Serial.print("With␣quadratic␣interpolation:␣");
71  Serial.print(duration_alg2);
72  Serial.println("␣us");
73  Serial.print("R1_alg2=␣");
74  Serial.println(Re_est_alg2,3);
75  Serial.print("R2_alg2=␣");
76  Serial.println(Ri_est_alg2,3);
77  Serial.print("C2_alg2=␣");
```

```
78   Serial.print(Cm_est_alg2*1e9,3);
79   Serial.println("␣nF");
80   Serial.print("Fc_alg2=␣");
81   Serial.println(p_interpolation/(2.0*PI),3);
82 }
83
84 void loop()
85 {
86 }
```

References

1. Abbasbandy S (2005) Extended Newton's method for a system of nonlinear equations by modified Adomian decomposition method. Applied Mathematics and Computation 170(1):648–656
2. Al-Ali A, Elwakil A, Maundy B, Freeborn T (2018) Extraction of phase information from magnitude-only bio-impedance measurements using a modified kramers–kronig transform. Circuits, Systems, and Signal Processing pp 1–16
3. Babolian E, Biazar J, Vahidi A (2004) Solution of a system of nonlinear equations by Adomian decomposition method. Applied Mathematics and Computation 150(3):847–854
4. Bertrand CA, Hopfer U (2002) Measurement of membrane capacitance in epithelial monolayers. In: Epithelial Cell Culture Protocols, Springer, pp 315–327
5. Blad B (1996) Clinical applications of characteristic frequency measurements: preliminaryin vivo study. Medical and Biological Engineering and Computing 34(5):362–365
6. Boinet M, Condolf C, Goulet R, Tribollet B, Vivier V (2016) Parameter identification in electrochemical impedance spectroscopy applications: Analysis of sensitivity. In: Meeting Abstracts, The Electrochemical Society, 23, pp 1707–1707
7. Bondarenko AS (2012) Analysis of large experimental datasets in electrochemical impedance spectroscopy. Analytica chimica acta 743:41–50
8. Boukamp BA, Rolle A (2018) Use of a distribution function of relaxation times (DFRT) in impedance analysis of SOFC electrodes. Solid State Ionics 314:103–111
9. Cordero A, Torregrosa JR (2007) Variants of Newton's method using fifth-order quadrature formulas. Applied Mathematics and Computation 190(1):686–698
10. Darvishi M, Barati A (2007) A third-order Newton-type method to solve systems of nonlinear equations. Applied Mathematics and Computation 187(2):630–635

11. De Lorenzo A, Andreoli A, Matthie J, Withers P (1997) Predicting body cell mass with bioimpedance by using theoretical methods: a technological review. Journal of Applied Physiology 82(5):1542–1558
12. Dong T, Kirchev A, Mattera F, Kowal J, Bultel Y (2011) Dynamic modeling of Li-ion batteries using an equivalent electrical circuit. Journal of the Electrochemical Society 158(3):A326–A336
13. Ferreira J, Seoane F, Ansede A, Bragos R (2010) Ad5933-based spectrometer for electrical bioimpedance applications. In: Journal of Physics: Conference Series, IOP Publishing, vol 224, p 012011
14. Ferreira J, Seoane F, Lindecrantz K (2013) Portable bioimpedance monitor evaluation for continuous impedance measurements. towards wearable plethysmography applications. In: 2013 35th Annual International Conference of the IEEE Engineering in Medicine and Biology Society (EMBC), IEEE, pp 559–562
15. Freeborn TJ, Elwakil AS, Maundy B (2017) Variability of cole-model bioimpedance parameters using magnitude-only measurements of apples from a two-electrode configuration. International Journal of Food Properties 20(sup1):S507–S519
16. Gheorghe A, Marin C, Constantinescu F, Nitescu M (2012) Parameter identification for a new circuit model aimed to predict body water volume. Advances in Electrical and Computer Engineering 12(4):83–86
17. Golbabai A, Javidi M (2007) A new family of iterative methods for solving system of nonlinear algebric equations. Applied Mathematics and Computation 190(2):1717–1722
18. Holevinsky KO, Nelson DJ (1998) Membrane capacitance changes associated with particle uptake during phagocytosis in macrophages. Biophysical journal 75(5):2577–2586
19. Hotka M, Zahradnik I (2014) Membrane capacitance changes due to temperature increase in rat cardiac myocytes. Biophysical Journal 106(2):121a–122a
20. Kern R, Sastrawan R, Ferber J, Stangl R, Luther J (2002) Modeling and interpretation of electrical impedance spectra of dye solar cells operated under open-circuit conditions. Electrochimica Acta 47(26):4213–4225
21. Kyle UG, Genton L, Slosman DO, Pichard C (2001) Fat-free and fat mass percentiles in 5225 healthy subjects aged 15 to 98 years. Nutrition 17(7-8):534–541
22. Macdonald JR, Barsoukov E (2005) Impedance spectroscopy: theory, experiment, and applications. History 1(8)
23. Manjakkal L, Cvejin K, Kulawik J, Zaraska K, Szwagierczak D, Socha RP (2014) Fabrication of thick film sensitive RuO_2-TiO_2 and Ag/AgCl/KCl reference electrodes and their application for pH measurements. Sensors and Actuators B: Chemical 204:57–67
24. Manjakkal L, Cvejin K, Bajac B, Kulawik J, Zaraska K, Szwagierczak D (2015) Microstructural, impedance spectroscopic and potentiometric analysis of Ta_2O_5 electrochemical thick film pH sensors. Electroanalysis 27(3):770–781

25. Manjakkal L, Djurdjic E, Cvejin K, Kulawik J, Zaraska K, Szwagierczak D (2015) Electrochemical impedance spectroscopic analysis of RuO_2 based thick film pH sensors. Electrochimica Acta 168:246–255
26. Maundy BJ, Elwakil AS, Allagui A (2015) Extracting the parameters of the single-dispersion cole bioimpedance model using a magnitude-only method. Computers and Electronics in Agriculture 119:153–157
27. Moss P, Au G, Plichta E, Zheng J (2008) An electrical circuit for modeling the dynamic response of Li-ion polymer batteries. Journal of The Electrochemical Society 155(12):A986–A994
28. Noor MA (2007) Fifth-order convergent iterative method for solving nonlinear equations using quadrature formula. J Math Control Sci Appl 1:241–249
29. Ortega JM, Rheinboldt WC (1970) Iterative solution of nonlinear equations in several variables, vol 30. Siam
30. Qiao G, Wang W, Duan W, Zheng F, Sinclair AJ, Chatwin CR (2012) Bioimpedance analysis for the characterization of breast cancer cells in suspension. IEEE Transactions on biomedical engineering 59(8):2321–2329
31. Ramírez-Chavarría RG, Quintana-Carapia G, Müller MI, Mattila R, Matatagui D, Sánchez-Pérez C (2018) Bioimpedance parameter estimation using fast spectral measurements and regularization. IFAC-PapersOnLine 51(15):521–526
32. Sanchez B, Schoukens J, Bragos R, Vandersteen G (2011) Novel estimation of the electrical bioimpedance using the local polynomial method. Application to in vivo real-time myocardium tissue impedance characterization during the cardiac cycle. IEEE Transactions on Biomedical Engineering 58(12):3376–3385
33. Sanchez B, Rojas CR, Vandersteen G, Bragos R, Schoukens J (2012) On the calculation of the D-optimal multisine excitation power spectrum for broadband impedance spectroscopy measurements. Measurement Science and Technology 23(8):085702
34. Sanchez B, Bandarenka AS, Vandersteen G, Schoukens J, Bragos R (2013) Novel approach of processing electrical bioimpedance data using differential impedance analysis. Medical Engineering and Physics 35(9):1349–1357
35. Sánchez Terrones B, Louarroudi E, Pintelon R, Bragós Bardia R (2013) Modeling the non-stationary behaviour of time-varying electrical bioimpedance. In: 19th IMEKO TC-4, 2013, July 18-19: Symposium Measurements of Electrical Quantities, Universitat Politècnica de Catalunya (UPC), pp 378–384
36. Santos-Sacchi J (2004) Determination of cell capacitance using the exact empirical solution of $\delta y/\delta cm$ and its phase angle. Biophysical journal 87(1):714–727
37. Schulz H, Teske D, Penven D, Tomczak J (2006) Fat-free mass from two prediction equations for bioelectrical impedance analysis in a large german population compared with values in swiss and american adults: Reasons for a biadata project. Nutrition 22(9):973

38. Seoane F, Ferreira J, Sanchéz JJ, Bragós R (2008) An analog front-end enables electrical impedance spectroscopy system on-chip for biomedical applications. Physiological measurement 29(6):S267
39. Simić M (2014) Complex impedance measurement system for environmental sensors characterization. In: Telecommunications Forum Telfor (TELFOR), 2014 22nd, IEEE, pp 660–663
40. Simić M, Stojanović GM (2017) Compact electronic system for complex impedance measurement and its experimental verification. In: Circuit Theory and Design (ECCTD), 2017 European Conference on, IEEE, pp 1–4
41. Simić M, Babić Z, Risojević V, Stojanović GM (2016) A novel non-iterative method for real-time parameter estimation of the Fricke-Morse model. Advances in Electrical and Computer Engineering 16(4):57–62
42. Simić M, Manjakkal L, Zaraska K, Stojanović GM, Dahiya R (2017) Tio_2-based thick film pH sensor. IEEE Sensors Journal 17(2):248–255
43. Vargas-Bernal R, Carlos A, Gómez-Polo C (2018) Electrical circuit modeling of sensor magneto-impedances with a square-root frequency dependence. IEEE Sensors Journal 18(2):623–628
44. Wang C, Nehrir MH, Shaw SR (2005) Dynamic models and model validation for PEM fuel cells using electrical circuits. IEEE transactions on energy conversion 20(2):442–451
45. Wang Z, Luo M, Geng Y, Lin B, Zhu Y (2018) A model to compare convective and radiant heating systems for intermittent space heating. Applied Energy 215:211–226
46. Ward L, Heitmann B (1998) Multiple frequency bioelectrical impedance analysis (mfbia) and rx plots in the assessment of obesity. Proc Aust Soc Study Obesity 7:20
47. Ward LC, Heitmann BL, Craig P, Stroud D, Azinge E, Jebb S, Cornish BH, Swinburn B, O'DEA K, Rowley K, et al. (2000) Association between ethnicity, body mass index, and bioelectrical impedance: Implications for the population specificity of prediction equations. Annals of the New York Academy of Sciences 904(1):199–202
48. Yousri D, AbdelAty AM, Said LA, AboBakr A, Radwan AG (2017) Biological inspired optimization algorithms for cole-impedance parameters identification. AEU-International Journal of Electronics and Communications 78:79–89